PCCP

Exciplex funnel resonances in chemical reaction dynamics: The nonadiabatic tunneling case associated with an avoided crossing at a saddle point

Ronald S. Friedman,[a] Thomas C. Allison[b]† and Donald G. Truhlar*[b]

[a] *Department of Chemistry, Indiana University Purdue University Fort Wayne, Fort Wayne, IN 46805-1499, USA*
[b] *Department of Chemistry and Supercomputer Institute, University of Minnesota, Minneapolis, MN 55455-0431, USA*

Received 2nd November 1998, Accepted 27th January 1999

We report quantum mechanical calculations on a one-dimensional model of a chemical reaction with an electronically excited exciplex funnel over the saddle point to study the competition between direct reflection from the upper diabat and metastable trapping (resonances). Particular emphasis is placed on the effect of the funnel on transition probabilities and delay times as a function of energy and as a function of the magnitude of the energy gap at the saddle point. Quantum dynamics calculations of energy-dependent transition probabilities for a series of energy gaps reveal a regime where the main effect is diabatic reflectivity in direct, short-lived collisions and another regime where the main effect is a series of collisional resonances.

I Introduction

Our fundamental understanding of electronically nonadiabatic reactions, *i.e.*, those occurring on coupled potential energy surfaces, is less fully developed than the theory of electronically adiabatic reactions occurring on a single surface. Electronically nonadiabatic reactions are often studied by photochemistry (electronically excited reactants) or chemiluminescence (electronically excited products). The study of such reactions by simulations involving converged quantum dynamics has become feasible in recent years.[1–4] An interesting phenomenon about which such calculations can provide new insight is the effect of a funnel[5,6] in a low-energy excited surface on the reaction probability of a ground-electronic-state reaction[4] or inelastic collision.[7] A particularly interesting case is where the minimum of the excited surface occurs at a geometry similar to the ground-state saddle point, a situation that might occur when the ground-state saddle point can be modeled as an avoided crossing of two diabatic valence bond configurations.[4,8,9] For example, the saddle point of $A + BC \rightarrow AB + C$ results from the interaction of the configurations $\phi_A \phi_B \phi_C(\alpha\beta - \beta\alpha)\alpha$ and $\phi_A \phi_B \phi_C \alpha(\alpha\beta - \beta\alpha)$, where ϕ_X is an atomic orbital on center X. The resulting energy gap between the adiabatic potential energy surfaces may be small if the rearrangement is disallowed by orbital symmetry[10] or orbital phase[11] considerations. If there is a small gap, a system approaching the saddle point on the lower surface may make a transition to the upper surface and reflect, resulting in a lower transmission coefficient. This has been postulated to occur in both electron transfer reactions[12] and Woodward–Hoffmann forbidden rearrangements[13] (the latter is a specific case where both surfaces are excited, but the idea is the same). For weak adiabatic coupling, a system, once excited, may actually be trapped in the funnel, forming a metastable system that can be called an exciplex funnel resonance[7] if it decays before a third-body collision or an exciplex funnel intermediate if it lives long enough to suffer collisions. So far there is no experimental evidence for funnel exciplexes associated with saddle point transit, but exciplex funnel resonances have been observed spectroscopically as predissociating states.[14]

Dating back to the first decade of quantum mechanics, there have been many studies of quantum mechanical nuclear motion in two coupled electronic states, especially by employing analytic and semiclassical methods for the analysis of scattering by coupled one-dimensional potential curves.[15] We draw the reader's attention to several studies of reduced-dimensionality systems that are especially relevant to the problem of a funnel over a saddle point. Baer and Child[16] studied resonances in one-dimensional model systems with an excited-state minimum over a ground-state barrier. Shin and Light[17] studied transmission probabilities in one-dimensional barrier problems in which an excited state has a minimum over the saddle point, and they also extended their study to a collinear three-body model with the lower surface similar to $H + H_2$ and again an excited-state minimum over the saddle point. Qi and Bowman[18] extended the study of the one-dimensional model system of Shin and Light to higher energies and observed funnel resonances for several values of the parameters. They found that making the region of strong electronic coupling narrower (in the reaction coordinate) or making the gap (in energy) smaller led to broader resonances. Zhu and Nakamura derived semiclassical formulas for the scattering matrix of two-state linear curve-crossing problems[19] as well as general two-state[20] and general multistate[21] curve-crossing problems. An especially interesting case they treated is the two-state case of a one-dimensional excited adiabatic potential having a minimum lying over the maximum of a lower adiabatic potential energy curve; they call this the nonadiabatic tunneling case.[19–22]

The work reported in the present paper was motivated by the observation of exciplex funnel resonances in three-

† Present address: Computational Chemistry Group, National Institute of Standards and Technology, 100 Bureau Drive, Stop 8380, Gaithersburg, MD 20899-8380, USA.

dimensional three-body model systems with the lower surface similar to $Cl + H_2$ and an excited-state surface having a minimum over the saddle point.[4] This may be called the avoided-crossing saddle-point case, or it may be called the nonadiabatic tunneling case, in analogy to the one-dimensional case treated by Zhu and Nakamura.[19–22] In order to better understand the quantum mechanical consequences of a funnel situated vertically over a saddle point, in this paper we will consider a sequence of one-dimensional model systems consisting of a lower adiabatic potential curve with a barrier, an upper adiabatic potential curve with a minimum representing the exciplex (excited-state funnel over the ground-state saddle point), and various magnitudes of the minimum adiabatic gap. We will systematically vary the parameters such that the gap E_{gap} over the saddle point takes on values in the range from 10 to 400 cm^{-1} (1.2–50 meV). We will then calculate accurate transmission probabilities, delay time matrix elements and lifetime matrix elements as functions of the total energy E of the collision. We will also calculate the complex energies of the poles of the scattering S matrix representing funnel resonances[7] as well as their partial widths. The effect of barrier resonances[23,24] will also be considered.

Section II presents the fundamental theory for scattering by coupled potential energy curves. Section III presents the computational methods used for calculating transmission probabilities, delay times and lifetime matrix elements as well as for locating S matrix poles. Section IV presents the model potential curves. Section V presents a discussion of the results of scattering calculations and resonance pole determinations for a range of energy gaps. Section VI contains concluding remarks.

II Theory

We consider the case of a particle moving in one dimension x governed by a 2×2 potential matrix. Our calculations are carried out in a diabatic representation in which the potential energy matrix is given by

$$\boldsymbol{V} = \begin{pmatrix} V_{11}(x) & V_{12}(x) \\ V_{21}(x) & V_{22}(x) \end{pmatrix} \tag{1}$$

where V_{11} and V_{22} are called the diabatic potentials, and V_{12} is called the diabatic coupling and is equal to V_{21} by hermiticity. The two-state problem has four channels labelled as follows: (1) state 1 at $x = +\infty$, (2) state 1 at $x = -\infty$, (3) state 2 at $x = +\infty$, and (4) state 2 at $x = -\infty$. The Schrödinger equation for this problem is

$$\frac{d^2\boldsymbol{Y}}{dx^2} + \frac{2\mu}{\hbar^2}(E\boldsymbol{I} - \boldsymbol{V})\boldsymbol{Y}(x) = 0 \tag{2}$$

where μ is the reduced mass, E is the scattering energy, $\boldsymbol{I}$ is the identity matrix, and $\boldsymbol{Y}$ is the column vector solution

$$\boldsymbol{Y} = \begin{pmatrix} Y_1 \\ Y_2 \end{pmatrix} \tag{3}$$

Let

$$\varepsilon_1 = V_{11}(x = +\infty) \tag{4a}$$

$$\varepsilon_2 = V_{11}(x = -\infty) \tag{4b}$$

$$\varepsilon_3 = V_{22}(x = +\infty) \tag{4c}$$

and

$$\varepsilon_4 = V_{22}(x = -\infty) \tag{4d}$$

We consider the curve-crossing case where $\varepsilon_1 \leq E \leq \varepsilon_3$ and $\varepsilon_4 \leq E \leq \varepsilon_2$. In this case the boundary conditions are

$$Y_1(x) \underset{x \to -\infty}{\sim} \frac{1}{\sqrt{k_2}}[A_{--}\exp(-k_2 x) + A_{-+}\exp(k_2 x)] \tag{5a}$$

$$Y_1(x) \underset{x \to +\infty}{\sim} \frac{1}{\sqrt{k_1}}[A_{+-}\exp(-ik_1 x) + A_{++}\exp(ik_1 x)] \tag{5b}$$

$$Y_2(x) \underset{x \to -\infty}{\sim} \frac{1}{\sqrt{k_4}}[B_{--}\exp(-ik_4 x) + B_{-+}\exp(ik_4 x)] \tag{5c}$$

$$Y_2(x) \underset{x +\infty}{\sim} \frac{1}{\sqrt{k_3}}[B_{+-}\exp(-k_3 x) + B_{++}\exp(k_3 x)] \tag{5d}$$

where the first subscript of each coefficient refers to the boundary ($x \to \pm\infty$), the second subscript refers to a positive or negative exponent in the exponential, and the asymptotic wavenumbers are given by

$$k_n = \sqrt{2\mu(E - \varepsilon_n)}/\hbar \tag{6a}$$

for open channels 1 and 4, and

$$k_n = \sqrt{2\mu(\varepsilon_n - E)}/\hbar \tag{6b}$$

for closed channels 2 and 3. In addition to the physical, real values of E, we will consider the analytic continuation to complex E. We will consider the case where $\varepsilon_4 = 0$ and $\varepsilon_4 < \varepsilon_1$. Then physical scattering energies have $E > 0$, and resonances lie in the fourth quadrant of the complex energy plane. When E is real, k_n is taken as the positive root; when E is in the fourth quadrant, then k_1 and k_4 are in the fourth quadrant and k_2 and k_3 are in the first quadrant.

Since only two of the channels are open, we focus on the 2×2 unitary scattering matrix $\boldsymbol{S}$, which relates the coefficients of the outgoing waves to the coefficients of the incoming waves:

$$\begin{pmatrix} A_{++} \\ B_{--} \end{pmatrix} = \begin{pmatrix} S_{11} & S_{14} \\ S_{41} & S_{44} \end{pmatrix} \begin{pmatrix} A_{+-} \\ B_{-+} \end{pmatrix} \tag{7}$$

Note that in the S matrix, the subscripts on the matrix elements do not indicate the row and column locations but rather are indices for channel designations. The transition probability for the transition from channel n to channel m is given by[25]

$$P_{nm} = |S_{mn}|^2 \tag{8}$$

The Schrödinger eqn. (2) can be solved at complex, as well as real, energies E. Quantum mechanical resonances correspond to poles in the S matrix at complex energies[26]

$$\bar{E} = E_R - i\Gamma/2 \tag{9}$$

where E_R is the real part of the resonance energy and Γ is the resonance width (real and positive by definition). For each resonance energy, all matrix elements S_{mn} have poles at $E = \bar{E}$. We search for poles in $\boldsymbol{S}$ by directly solving eqn. (2) at complex energies, as was done previously.[24,27]

To characterize a resonance, we use the lifetime matrix $\boldsymbol{Q}$ and the delay-time matrix $\boldsymbol{\Delta t}$, whose elements are given by[28]

$$Q_{nm} = i\hbar \sum_l S_{nl}(dS^*_{ml}/dE) \tag{10}$$

and

$$\Delta t_{nm} = \mathrm{Im}\left(\hbar(S_{mn})^{-1}\frac{dS_{mn}}{dE}\right) \tag{11}$$

The eigenvalues q_{nn} of the lifetime matrix can be associated with the exponental decay times of (long-lived) metastable states when the values of q_{nn} are large.[28] The channel-to-

channel delay time Δt_{nm} represents the time difference between a pulse being injected into channel n and a pulse appearing in channel m, relative to the same time difference in the absence of a potential. At real energies E in the proximity of E_R, the scattered particle will experience a delay time, which is large if the resonance width Γ is small.

In the vicinity of an isolated resonance, the scattering matrix element S_{mn} can be written[26,29]

$$S_{mn}(E) = S^0_{mn}(E) - \mathrm{i}\,\frac{\gamma_m \gamma_n}{E - E_R + \mathrm{i}\Gamma/2} \tag{12}$$

where $S^0_{mn}(E)$ is the nonresonant background contribution to the scattering matrix element, and γ_n is the partial width amplitude for channel n. In the case of an isolated, narrow resonance (INR) for which γ_n, γ_m, and S^0_{mn} are independent of energy and S^0_{mn} is a negligible contributor to S_{mn}, one can show that the delay time has a maximum at $E = E_R$, at which

$$\Delta t_{nm}\,\Gamma = 2\hbar \tag{13}$$

In addition, for a single-channel mechanical system having an INR centered at E_R, the 1×1 collision matrix $\boldsymbol{Q}$ is given by[28]

$$Q(E_R)\Gamma = 4\hbar \tag{14}$$

The "partial width" Γ_n for either entering the metastable resonance from channel n or leaving the resonance to go into channel n is given by $|\gamma_n|^2$. For an INR, it has been shown that[26,29]

$$\sum_n \Gamma_n = \Gamma \tag{15}$$

and practical experience shows that this equality is a sensitive test of whether a resonance may be treated as an INR.[30]

III Computational methods

We seek the solution $\boldsymbol{Y}$ to eqn. (2) subject to the boundary conditions [eqn. (5a)–(5d)]. We consider problems where the diabatic potentials decay to their asymptotic values exponentially fast, and the diabatic coupling decays to zero exponentially. In such cases it is reasonable to assume that eqn. (5b) and (5d) hold to within an acceptable numerical accuracy for $x \geq x_2$, and that eqn. (5a) and (5c) hold to within acceptable numerical accuracy for $x \leq -x_1$, where x_1 and x_2 are positive numbers. All numerical results must be converged with respect to increasing x_1 and x_2.

We consider the case in which channel 1 is the incident channel; therefore, $B_{-+} = 0$. We also require that $Y_1(-x_1)$ and $Y_2(x_2)$ be well-behaved; therefore, $A_{--} = B_{++} = 0$. The boundary conditions therefore become

$$\boldsymbol{Y} \underset{x\to-\infty}{\sim} \begin{pmatrix} \dfrac{1}{\sqrt{k_2}}\,[A_{-+}\exp(k_2 x)] \\ \dfrac{1}{\sqrt{k_4}}\,[B_{--}\exp(-ik_4 x)] \end{pmatrix} \tag{16a}$$

$$\boldsymbol{Y} \underset{x\to+\infty}{\sim} \begin{pmatrix} \dfrac{1}{\sqrt{k_1}}\,[A_{+-}\exp(-ik_1 x) + A_{++}\exp(ik_1 x)] \\ \dfrac{1}{\sqrt{k_3}}\,[B_{+-}\exp(-k_3 x)] \end{pmatrix} \tag{16b}$$

Since the ratio of the coefficents A_{-+} and B_{--} is as yet undetermined, we do not know *a priori* the solution vector $\boldsymbol{Y}$ at $x = -x_1$. Therefore, we can not directly propagate $\boldsymbol{Y}$ from $-x_1$ to x_2. Instead, we consider two linearly independent solutions, $\boldsymbol{Y_a}$ and $\boldsymbol{Y_b}$, which satisfy the boundary conditions

$$\boldsymbol{Y_a} \underset{x\to-\infty}{\sim} \begin{pmatrix} \dfrac{1}{\sqrt{k_2}}\exp(k_2 x) \\ 0 \end{pmatrix} \tag{17a}$$

$$\boldsymbol{Y_b} \underset{x\to-\infty}{\sim} \begin{pmatrix} 0 \\ \dfrac{1}{\sqrt{k_4}}\,[\exp(-ik_4 x)] \end{pmatrix} \tag{17b}$$

The desired solution is

$$\boldsymbol{Y} = A_{-+}\boldsymbol{Y_a} + B_{--}\boldsymbol{Y_b} \tag{18}$$

which has the correct $x \to -\infty$ asymptotic behavior of eqn. (16a). The linearly independent solutions $\boldsymbol{Y_a}$ and $\boldsymbol{Y_b}$ are numerically propagated from $x = -x_1$ to $x = x_2$ with stepsize Δx using a numerical integrator.

To ensure that the two numerical solutions remain linearly independent, we invoke the Gram–Schmidt orthonormalization procedure[31] on the 4×2 matrix

$$\boldsymbol{Z}(x, x+\Delta x) = \begin{pmatrix} \boldsymbol{Y_a}(x+\Delta x) & \boldsymbol{Y_b}(x+\Delta x) \\ \boldsymbol{Y_a}(x) & \boldsymbol{Y_b}(x) \end{pmatrix} \tag{19}$$

in which the first column vector of $\boldsymbol{Z}$ is normalized, and the second column vector is made orthogonal to the first normalized column vector and then is itself normalized.

The $x \to +\infty$ asymptotic forms of the two solutions can be written in general as

$$\boldsymbol{Y_a} \underset{x\to+\infty}{\sim} \begin{pmatrix} \dfrac{1}{\sqrt{k_1}}\,[a_{+-}(1)\exp(-ik_1 x) + a_{++}(1)\exp(ik_1 x)] \\ \dfrac{1}{\sqrt{k_3}}\,[b_{+-}(1)\exp(-k_3 x) + b_{++}(1)\exp(k_3 x)] \end{pmatrix} \tag{20a}$$

$$\boldsymbol{Y_b} \underset{x\to+\infty}{\sim} \begin{pmatrix} \dfrac{1}{\sqrt{k_1}}\,[a_{+-}(2)\exp(-ik_1 x) + a_{++}(2)\exp(ik_1 x)] \\ \dfrac{1}{\sqrt{k_3}}\,[b_{+-}(2)\exp(-k_3 x) + b_{++}(2)\exp(k_3 x)] \end{pmatrix} \tag{20b}$$

where (1) and (2) on the coefficients correspond to the first and second linearly independent solutions, respectively. By using the values of $\boldsymbol{Y_a}$ and $\boldsymbol{Y_b}$ at both $x = x_2$ and $x = x_2 - \Delta x$ obtained *via* numerical integration, we can obtain the eight coefficients shown in eqn. (20a)–(20b). The desired linear combination, eqn. (18), has the $x \to +\infty$ asymptotic form

$$\boldsymbol{Y} \sim \begin{pmatrix} \dfrac{1}{\sqrt{k_1}}\,[(A_{-+}a_{+-}(1) + B_{--}a_{+-}(2))\mathrm{e}^{-ik_1 x} \\ \qquad + (A_{-+}a_{++}(1) + B_{--}a_{++}(2))\mathrm{e}^{ik_1 x}] \\ \dfrac{1}{\sqrt{k_3}}\,[(A_{-+}b_{+-}(1) + B_{--}b_{+-}(2))\mathrm{e}^{-k_3 x} \\ \qquad + (A_{-+}b_{++}(1) + B_{--}b_{++}(2))\mathrm{e}^{k_3 x}] \end{pmatrix} \tag{21}$$

which implies that [see eqn. (16b)]

$$A_{+-} = A_{-+}a_{+-}(1) + B_{--}a_{+-}(2) \tag{22a}$$

$$A_{++} = A_{-+}a_{++}(1) + B_{--}a_{++}(2) \tag{22b}$$

$$B_{+-} = A_{-+}b_{+-}(1) + B_{--}b_{+-}(2) \tag{22c}$$

$$0 = A_{-+}b_{++}(1) + B_{--}b_{++}(2) \tag{22d}$$

From eqn. (22d), we compute the ratio, R, defined as

$$R = \frac{B_{--}}{A_{-+}} = -\frac{b_{++}(1)}{b_{++}(2)} \tag{23}$$

From R we can determine the matrix elements S_{m1} for scattering from incident channel 1. In particular, the scattering matrix elements are given by

$$S_{11} = \frac{A_{++}}{A_{+-}} = \frac{A_{-+}a_{++}(1) + B_{--}a_{++}(2)}{A_{-+}a_{+-}(1) + B_{--}a_{+-}(2)}$$

$$= \frac{a_{++}(1) + Ra_{++}(2)}{a_{+-}(1) + Ra_{+-}(2)} \tag{24a}$$

$$S_{41} = \frac{B_{--}}{A_{+-}} = \frac{B_{--}}{A_{-+}a_{+-}(1) + B_{--}a_{+-}(2)}$$

$$= \frac{R}{a_{+-}(1) + Ra_{+-}(2)} \tag{24b}$$

Scattering matrix elements are obtained using the matrix Numerov integrator[32] which propagates both linearly independent solutions $\boldsymbol{Y_a}$ and $\boldsymbol{Y_b}$ simultaneously; we typically use $x_1 = x_2 = 12\,a_0$ and $\Delta x = 5.0 \times 10^{-4}\ a_0$. The values of x_1 and x_2 required for convergence are reduced to $12\ a_0$ by using the local wavenumbers, $\sqrt{2\mu[E-V(x)]}$ and $\sqrt{2\mu[V(x)-E]}$, rather than the asymptotic wavenumbers [eqn. (6a)–(6b)] in the boundary conditions.

The Gram–Schmidt procedure is performed at every integration point; *i.e.* for all matrices $\boldsymbol{Z}$, including $\boldsymbol{Z}(-x_1, -x_1 + \Delta x)$ but excluding $\boldsymbol{Z}(x_2 - \Delta x, x_2)$. By maintaining linear independence of the two propagated solution vectors, we are able to obtain matrix elements S_{11} converged to better than 0.1%. However, because of the Gram–Schmidt procedure, we can no longer directly compare the magnitudes of the solution vectors at $x = +\infty$ to those at $x = -\infty$, and therefore, attempts to get converged values of S_{41} *via* eqn. (24b) were not successful. Therefore, another procedure is used, as described below.

Before we discuss the procedure for determining S_{41}, we discuss the calculation of S_{44} (since, as we will see, it is needed for computing S_{41}). To compute S_{44}, we use exactly the same algorithm as described in this section for computing S_{11} but instead of the diabatic potential matrix $\boldsymbol{V}$ of eqn. (1), we use the modified potential matrix $\boldsymbol{V}_{\mathrm{mod}}$ given by

$$\boldsymbol{V}_{\mathrm{mod}}(x) = \begin{pmatrix} V_{22}(-x) & V_{12}(-x) \\ V_{12}(-x) & V_{11}(-x) \end{pmatrix} \tag{25}$$

When the Schrödinger eqn. (2) is solved with the potential $\boldsymbol{V}_{\mathrm{mod}}$, the quantity computed by eqn. (24a) will be S_{44}. Although the matrix elements S_{11} and S_{44} are not, in general, equal, the symmetry of the scattering matrix requires that $P_{11} = P_{44}$, which was confirmed numerically using the computed values of S_{11} and S_{44}.

By using the fact that $\boldsymbol{S}$ is symmetric and unitary, it can be shown that, to within a multiplicative factor of ± 1,

$$S_{41} = FG + \mathrm{i}F \tag{26}$$

where

$$F = \pm\sqrt{(1 - P_{11})/(1 + G^2)} \tag{27a}$$

$$G = -\left(\frac{\mathrm{Im}(S_{11}) + \mathrm{Im}(S_{44})}{\mathrm{Re}(S_{11}) + \mathrm{Re}(S_{44})}\right) \tag{27b}$$

Therefore, S_{41} is known to within a real phase factor. The phase ambiguity is resolved in the following manner. First, the scattering matrix element S_{41} and its phase were computed using the positive root in eqn. (27a). Then we empirically determined a triad of energies $E_{1,2,3}$ for which the phase of S_{41} changed from slightly less than π at E_1 and E_2 to slightly greater than zero at E_3. Over the entire energy range studied, this situation occurred three times for each potential matrix $\boldsymbol{V}$. Each time this occurred, we fixed the phase of S_{41} by multiplying the matrix element by -1 for all energies $E \geq E_3$. The second modification needed occurred in the vicinity of the resonance energy E_{R}. Since, as we will discuss below, P_{14} goes through a zero at $E = E_{\mathrm{R}}$, there must be a simultaneous sign change in both the real and imaginary components of $S_{41}(E)$ as we traverse the resonance energy. Having already found E_{R} from analyses of the poles of S_{11} and S_{44}, we know precisely where the simultaneous sign changes in the real and imaginary parts of S_{41} are required. By taking $S_{14} = S_{41}$, we now have the complete S matrix.

The computational program for numerically determining $S_{11}(E)$ was tested with the model potentials from ref. 18. The reaction probabilities and resonance energies computed *via* this program are in agreement with the results of that reference.

All the dynamical quantities of interest are computed from the S matrix. Scattering calculations are performed at 54 001 energies equally spaced from 0.006 E_{h} (0.16 eV) to 0.06 E_{h} (1.6 eV), the energy interval being $\Delta E = 10^{-6}\ E_{\mathrm{h}}$ (0.027 meV). (Note that $E_{\mathrm{h}} = 1$ hartree.) Transition probabilities P_{nm} are computed at real energies E using eqn. (8). The small magnitude of ΔE is necessary to ensure the accuracy of finite difference calculations of the derivatives of the scattering matrix elements needed in eqn. (10) and (11) for the matrices $\boldsymbol{Q}$ and $\Delta\boldsymbol{t}$. Delay times Δt_{nm} are determined at real energies as previously described.[24] In particular, scattering matrix elements are fit at three consecutive energy values to the form

$$S_{mn}(E) = (c_1 + c_2 E + c_3 E^2) \times \exp[\mathrm{i}(c_4 + c_5 E + c_6 E^2)] \tag{28}$$

where c_k are real fitting parameters. Then the delay time at the central energy of the triad is obtained by

$$\Delta t_{nm}(E) = \hbar(c_5 + 2c_6 E) \tag{29}$$

For the lifetime matrix elements, in order to numerically obtain a *hermitian* matrix $\boldsymbol{Q}$ and *real* eigenvalues q_{nn}, we moved beyond a three-point fit of scattering matrix elements to a five-point fit, yielding more accurate numerical derivatives of $\boldsymbol{S}$. The derivative of the scattering matrix element at the central energy of the pentad is given by

$$\frac{dS^*_{ml}}{\mathrm{d}E}(E) = \frac{S^*_{ml}(E-2\Delta E) - 8S^*_{ml}(E-\Delta E) + 8S^*_{ml}(E+\Delta E) - S^*_{ml}(E+2\Delta E)}{12\Delta E} \tag{30}$$

The eigenvalues q_{nn} are easily obtained from the well-known analytical formula for the eigenvalues of a 2×2 matrix. Since the eigenvalues of $\boldsymbol{Q}$ should be real, as a measure of the degree of hermiticity of the numerical lifetime matrix, we computed from $q_{nn}(E)$ the ratio of its imaginary to real part, $\mathrm{Im}(q_{nn})/\mathrm{Re}(q_{nn})$. For the energy range from 0.01 E_{h} (0.27 eV) to 0.06 E_{h} (1.6 eV), in which two funnel resonances are found and in which all local maxima in $q_{\mathrm{nn}}(E)$ appear, the maximum value of this ratio is 3×10^{-6}.

Poles of the scattering matrix corresponding to resonances are located by numerically searching for zeroes in $1/S_{11}$ and $1/S_{44}$ at complex scattering energies. This procedure has been previously described.[24] In brief, we use a modified form of the International Mathematical and Statistical Library subroutine ZANLY, which utilizes Muller's method[33] to quadratically interpolate among three energy values to get the next estimate of the root. The root-finding algorithm is stopped when the relative difference between two approximate successive roots is within a parameter ERRREL, which we typically set to 10^{-10}. The values of Γ and E_{R} are converged with respect to numerical integration parameters to at least eight significant figures.

To confirm that indeed we have found first order poles of the scattering matrix and to determine partial widths of the resonances, we compute $(E-\bar{E})S_{mn}$ for many complex energies in the vicinity of $\bar{E}$. For an isolated resonance, at complex energies very close to $\bar{E}$ (such that the background contribution S^0_{mn} is negligible), we see from eqn. (12) that

$$(E-\bar{E})S_{mn}(E) = -i\gamma_m\gamma_n \tag{31}$$

Therefore, for first order poles and E close to the resonance energy, the above product should be approximately constant and should be equal to the residue at the pole. For all the funnel resonances identified in the present study, we were able to find square paths in the complex energy plane around $\bar{E}$ for which the calculated value of the product is constant to at least four significant figures. From the residues for S_{11} [S_{44}], the partial width amplitudes γ_1 [γ_4] and partial widths Γ_1 [Γ_4] of each resonance are determined.

IV Potentials

We study the two-state chemical reaction whose ground state is similar to $Cl + H_2$ and for which accurate three-dimensional quantum mechanical calculations on coupled diabatic potential energy surfaces have recently been performed.[4] In the three-dimensional studies, the lower adiabatic surface was very similar to the G3 potential energy surface;[9] the excited adiabatic surface had a broad minimum (a funnel) in the saddle point region of the lower surface. The scattering calculations utilized diabatic surfaces and, in particular, five sets of coupled diabats were used, such that the gap (*i.e.*, the minimum separation) of the corresponding adiabats ranged from 10 to 400 cm^{-1}. The five surface sets were designated I–V, and we will use the same designations here.

In our study, we use one-dimensional potential functions to model the three-dimensional diabatic surfaces along the collinear minimum enegy path (MEP). The variable x represents the reaction coordinate with $x = 0$ at the saddle point of the ground-state adiabat. Fig. 1(a), (b) and (c) show, respectively, the two adiabats, the two diabats, and the diabatic coupling along the MEP for case V of ref. 4 in which the adiabatic energy gap was 400 cm^{-1}. We describe below the one-dimensional functional forms we use to represent the potentials in Fig. 1 (as well as those for cases I–IV).

The potential energy function for the ground-state ClH_2 adiabatic curve is taken to be an unsymmetric Eckart function of the form

$$V_1^{ad}(x) = \frac{V_1 e^{\beta_1(x-x_1)}}{(1+e^{\beta_1(x-x_1)})^2} + \frac{V_2 e^{\beta_1(x-x_1)}}{(1+e^{\beta_1(x-x_1)})} \tag{32}$$

and the values of the numerical parameters, given in Table 1, are chosen so that the asymptotes match those of the ClH_2 G3 surface and the potential has a maximum value of $V_1^{ad,\,max} = 0.012584458\ E_h$ (0.34244067 eV or 2761.9693 cm^{-1}) at $x = 0$ in agreement with the value along the MEP of the G3 surface. The potential is shown in Fig. 2. Note that the $x \to -\infty$ asymptote of V_1^{ad} sets the zero of energy for the scattering calculations.

Table 1 Values (in atomic units) of parameters in potential energy functions[a]

For V_1^{ad}:
$V_1 = 4.0167971782296 \times 10^{-2}$
$\beta_1 = 5.5$
$x_1 = -4.364721325998 \times 10^{-2}$
$V_2 = 4.79833373 \times 10^{-3}$

For V_2^{ad}:
$V_{asym} = 3.61196179 \times 10^{-1}$
$V_3 = 9.8998917754 \times 10^{-1}$
$\beta_2 = 4.9818195151$
$x_2 = 5.0012635420 \times 10^{-2}$
$V_4 = 1.122019 \times 10^{-2}$
$V_5 = 7.9781762366 \times 10^{-1}$
$\beta_3 = 2.3471780470$
$x_3 = -7.6042693477 \times 10^{-1}$

For V_{12}:
$\beta_4 = 1.0487590725$
$x_4 = 8.1790045179 \times 10^{-1}$

[a] 1 E_h = 27.2113961 eV = 219474.63 cm^{-1}

The potential energy function for the excited-state ClH_2 adiabatic curve is of the form

$$V_2^{ad}(x) = V_{asym} - \frac{V_3 e^{\beta_2(x-x_2)}}{(1+e^{\beta_2(x-x_2)})^2} - \frac{V_4 e^{\beta_2(x-x_2)}}{(1+e^{\beta_2(x-x_2)})} - \frac{V_5 e^{\beta_3(x-x_3)}}{(1+e^{\beta_3(x-x_3)})^2} - V_{lower} \tag{33}$$

with the values of the numerical parameters also given in Table 1. When $V_{lower} = 0$, this potential function, also shown in Fig. 2, is representative of the upper adiabat for case V of ref. 4 and it has asymptotes of V_{asym} at $x = -\infty$ and $V_{asym} - V_4$ at $x = +\infty$. The potential of eqn. (33) has a minimum at $x = 0$ which, depending on the value of V_{lower}, can range from 10 to 400 cm^{-1} greater than $V_1^{ad,\,max}$, the maximum of the ground-state adiabat. The values of V_{lower} and the corresponding gaps between the saddle point maximum in V_1^{ad} and the funnel minimum in V_2^{ad} are given in Table 2. As seen, we have successfully provided one-dimensional potential functions that model the three-dimensional potential energy surfaces of ref. 4 along the MEP. The case labels in Table 2

Table 2 Case labels, V_{lower} values and adiabatic gaps

Case	V_{lower}/E_h	E_{gap}/cm^{-1}
I	1.777×10^{-3}	10.99
II	1.367×10^{-3}	100.97
III	9.11267×10^{-4}	200.99
IV	4.5563×10^{-4}	300.99
V	0	400.99

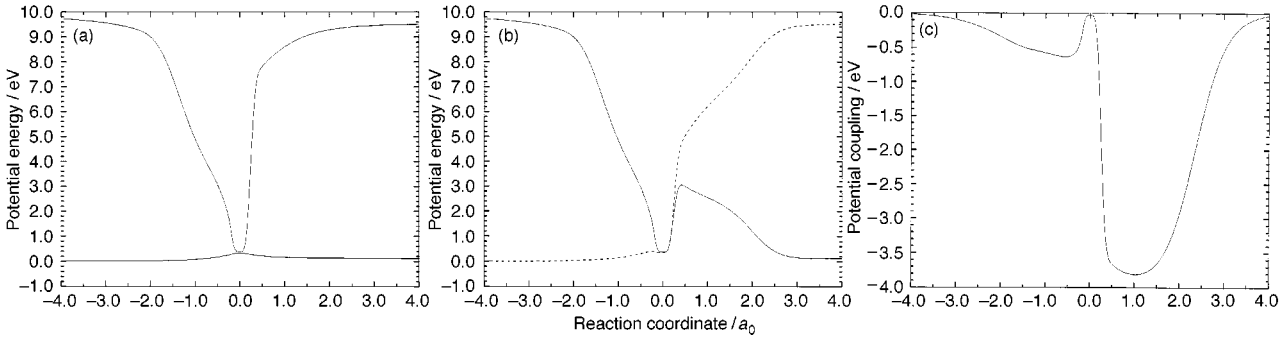

Fig. 1 Energies of the ClH_2 potential surfaces along the minimum energy path for case V of ref. 4. (a) Ground- and excited-state adiabatic potentials; (b) diabatic potentials; (c) diabatic coupling.

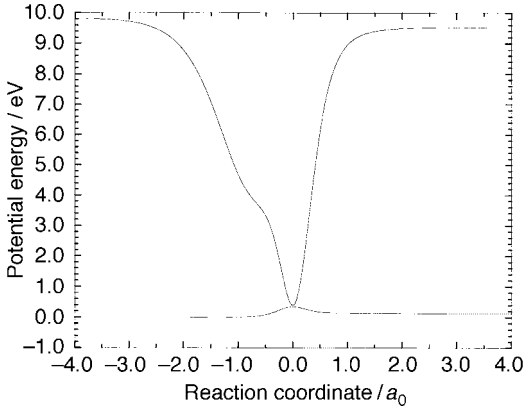

Fig. 2 One-dimensional adiabatic potentials V_1^{ad} and V_2^{ad} for case V (in which the gap is 400 cm^{-1}).

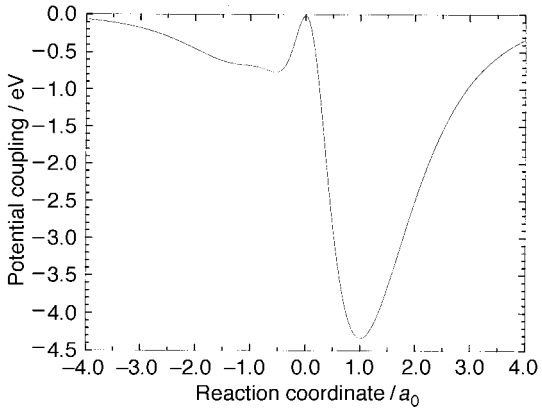

Fig. 3 One-dimensional diabatic coupling V_{12} used for all cases in the present study.

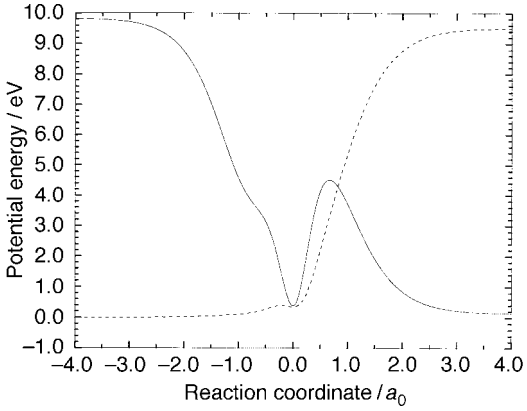

Fig. 4 One-dimensional diabatic potentials V_{11} (solid curve) and V_{22} (dotted curve) for case V.

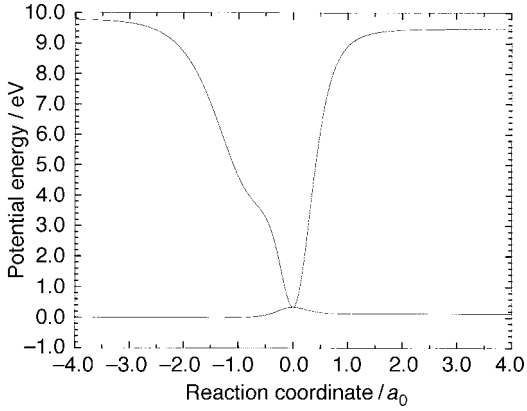

Fig. 5 Same as Fig. 2 but for case I (in which the gap is 10 cm^{-1}).

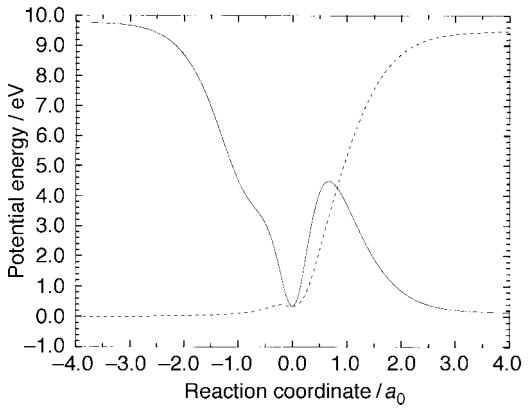

Fig. 6 Same as Fig. 4 but for case I.

follow those used in that earlier reference.

For the diabatic coupling, we use the functional form[17,18]

$$V_{12}(x) = -\sqrt{f(1-f)}(V_2^{ad} - V_1^{ad}) \quad (34)$$

where

$$f(x) = \tfrac{1}{2}[1 - \tanh(\beta_4(x - x_4))] \quad (35)$$

with the numerical parameters given in Table 1. The coupling is shown in Fig. 3. The corresponding diabatic potential energy functions are then given by

$$V_{11}(x) = (1-f)V_1^{ad} + fV_2^{ad} \quad (36a)$$

$$V_{22}(x) = fV_1^{ad} + (1-f)V_2^{ad} \quad (36b)$$

Fig. 4 shows the two diabatic curves for case V.

For all five cases (I–V), the same diabatic coupling V_{12} and ground-state adiabat V_1^{ad} are employed in the scattering calculations; V_{11} and V_{22} vary from case to case depending on the value of V_{lower} chosen for $V_2^{ad}(x)$. The adiabatic and diabatic potential curves for case I are depicted in Fig. 5 and 6, respectively.

We note here in passing that attempts to first find simple functional forms for the ClH_2 diabatic potential curves of ref. 4 were unsuccessful in that they did not yield adiabatic potentials that are smooth. Therefore, we fit the adiabats as above and then using the fit for the diabatic coupling, we immediately obtained the diabats *via* eqn. (36a)–(36b).

V Results and discussion

The Schrödinger eqn. (2) is solved in the diabatic basis using a reduced mass of 3474.057 m_e corresponding to $^{35}ClH_2$. Scattering calculations are performed at real energies in the range from 0.16 to 1.6 eV. The three-dimensional calculations of ref. 4 considered energies from 0.4 to 1.0 eV and characterized one funnel resonance. By extending the range of energies, we will locate two funnel resonances in the one-dimensional calculations.

Transition probabilities $P_{11} = P_{44}$ are shown in Fig. 7(a) and (b) for cases I and V, respectively. (It is not necessary to show $P_{14} = P_{41} = 1 - P_{11}$.) Delay times Δt_{nm} are shown in Fig. 8 and 9 for these two cases as well. Eigenvalues q_{nn} of the Q matrix as well as the trace of $\boldsymbol{Q}$ are shown in Fig. 10 and 11 for these same cases. Results for cases II–IV are similar and, therefore, are not plotted.

All of the delay time curves show three peaks; in Table 3, we give the values of the local maxima in Δt_{nm} and the corresponding energies. Similarly, all of the plots of the trace of the Q matrices have three peaks. In Table 4, we give the values of the local maxima in Tr(Q) and the energies, called E_{max}, at which these maxima occur; we also give the individual values of the eigenvalues at these energies.

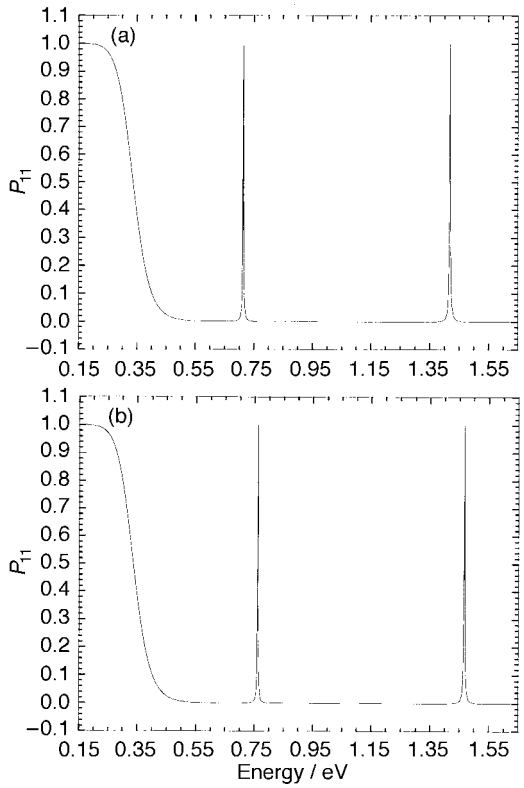

Fig. 7 Transition probability P_{11} as a function of scattering energy for (a) case I and (b) case V.

For each of the five cases I–V, we have found and characterized two resonances by performing scattering calculations at complex energies. We will denote the resonance with the lower (higher) value of E_R as funnel resonance 1(2). In Table 5, we present the resonance parameters E_R and Γ, as well as the partial widths Γ_1 and Γ_4. The value of E_R is given with

Table 3 Local maxima in the delay times Δt_{nm} at energies E^{nm}_{max}

Case	E^{11}_{max}/ eV	Δt_{11}/ fs	E^{14}_{max}/ eV	Δt_{14}/ fs	E^{44}_{max}/ eV	Δt_{44}/ fs
I	0.33467	9.087	0.33239	9.033	0.32991	8.990
	0.71280	513.07	0.71280	514.01	0.71280	514.95
	1.4186	388.66	1.4186	388.41	1.4186	388.15
II	0.33465	9.087	0.33233	9.032	0.32988	8.990
	0.72399	520.80	0.72399	521.68	0.72399	522.55
	1.4298	395.17	1.4298	394.92	1.4298	394.66
III	0.33465	9.085	0.33236	9.032	0.32991	8.990
	0.73639	529.84	0.73639	530.65	0.73639	531.47
	1.4422	402.58	1.4422	402.32	1.4422	402.06
IV	0.33467	9.085	0.33233	9.031	0.32991	8.990
	0.74883	539.35	0.74883	540.11	0.74883	540.86
	1.4546	410.17	1.4546	409.92	1.4546	409.66
V	0.33467	9.084	0.33236	9.031	0.32994	8.990
	0.76124	549.24	0.76124	549.94	0.76124	550.64
	1.4670	417.97	1.4670	417.71	1.4670	417.52

Table 4 Local maxima in the trace of $\boldsymbol{Q}$ at energies E_{max} and eigenvalues at E_{max}

Case	E_{max}/ eV	Trace $\boldsymbol{Q}$/ fs	q_{11}/ fs	q_{22}/ fs
I	0.33239	18.066	14.972	3.094
	0.71280	1028.18	1026.77	1.402
	1.4186	776.88	776.48	0.399
II	0.33233	18.065	14.972	3.093
	0.72399	1043.51	1042.16	1.355
	1.4298	789.90	789.51	0.393
III	0.33236	18.064	14.972	3.092
	0.73639	1061.48	1060.17	1.306
	1.4422	804.71	804.32	0.388
IV	0.33233	18.063	14.972	3.091
	0.74883	1080.39	1079.13	1.260
	1.4546	819.91	819.53	0.382
V	0.33236	18.061	14.972	3.090
	0.76124	1100.07	1098.86	1.217
	1.4670	835.51	835.13	0.377

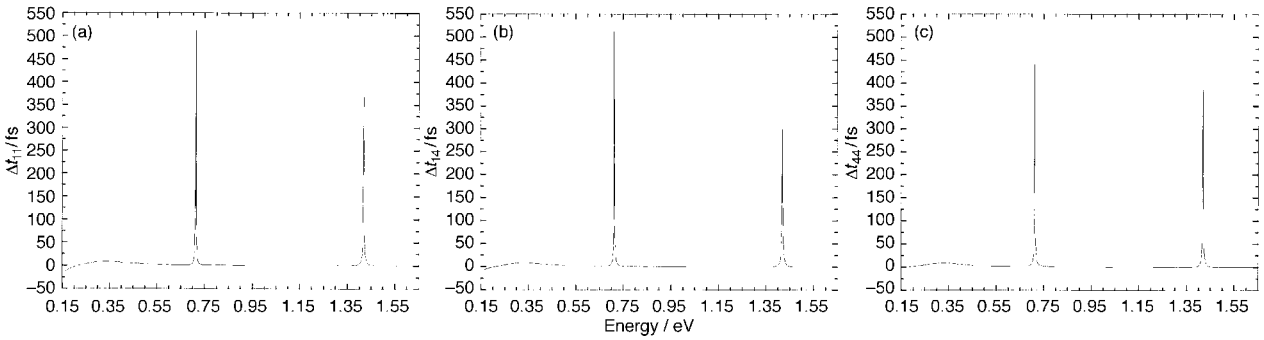

Fig. 8 Delay time matrix elements Δt_{nm} as a function of energy for case I; (a) Δt_{11}; (b) Δt_{14}; (c) Δt_{44}.

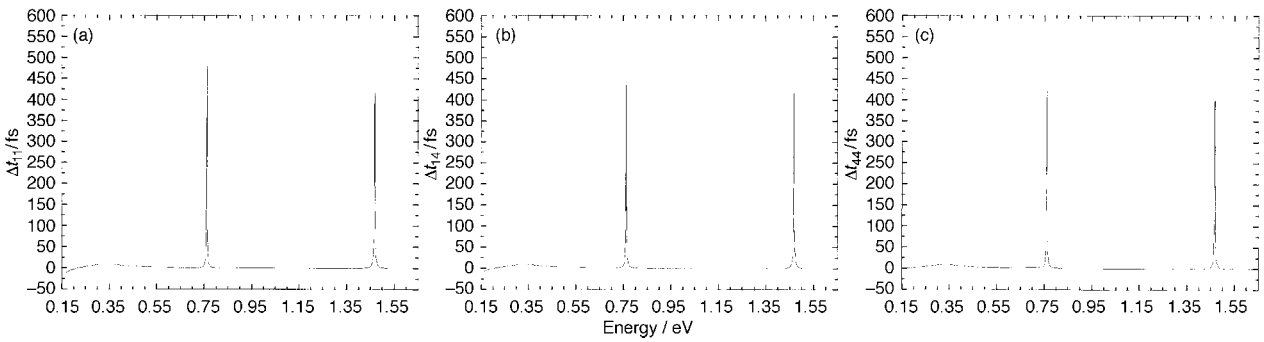

Fig. 9 Same as Fig. 8 but for case V.

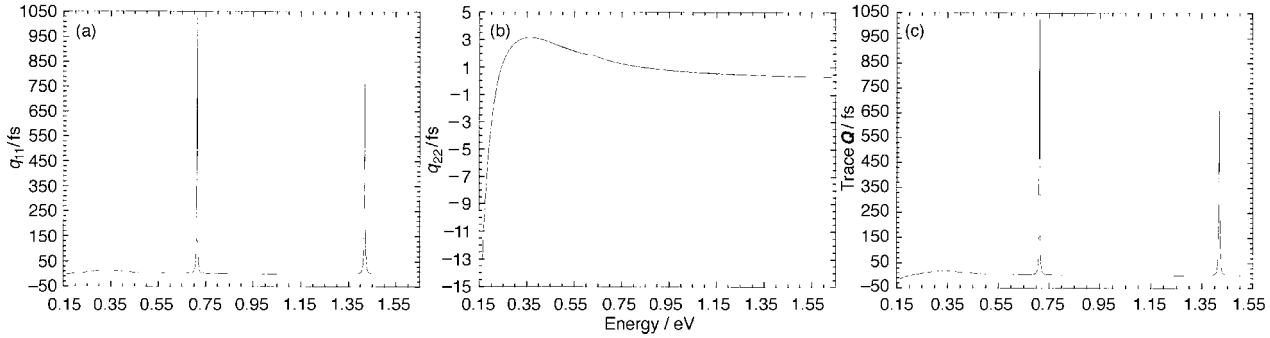

Fig. 10 Eigenvalues and trace of the lifetime matrix $\boldsymbol{Q}$ as a function of energy for case I; (a) eigenvalue q_{11}; (b) eigenvalue q_{22}; (c) trace of $\boldsymbol{Q}$.

respect to the maximum in the ground-state adiabatic curve; recall that this maximum has the same value in all five cases. Funnel resonance 1 is narrower by about 25% than funnel resonance 2; this is consistent with the former lying deeper within the well of the excited-state adiabatic curve. For a given funnel resonance, as we proceed from case I through to case V, the value of E_R increases; furthermore, the magnitude of this increase is remarkably close to the change in the value of V_{lower} and the adiabatic gap from case to case. In addition, for a given funnel resonance, the width slightly decreases as we move from case I to case V; the larger the adiabatic gap, the narrower (and longer-lived) is the metastable state, consistent with earlier results.[18] The observation that the width of a given funnel resonance does not change very much as we proceed from case I to case V can be understood in terms of the golden rule. Since the coupling in the diabatic representation is relatively strong (compare the magnitude of the diabatic coupling V_{12} to the values of the potential energies V_{11} and V_{22}), the coupling in the adiabatic representation is relatively weak. Since the latter coupling is weak, the decay of the funnel resonance should be described approximately by the golden rule,[34] in which case the width is proportional to the square of the adiabatic coupling matrix element. In the simplest possible application of this rule, we approximate the nuclear-motion matrix element by the value of the (diabatic) electronic coupling near the center of the funnel. Since the diabatic coupling is the same in all cases I to V, we expect the resonance width to show little variation.

Table 5 also presents, for each funnel resonance, the ratio of the sum of the partial widths to the total width. This ratio in all cases is very close to unity; the funnel resonances can indeed be considered ideal narrow resonances [see eqn. (15)].

As seen in Fig. 7, the transition probability P_{11} smoothly decreases from 1 to 0 as the energy approaches and surpasses $V_1^{ad,\,max}$. In fact, this initial decrease is, to within plotting accuracy, indistinguishable for the two cases shown (and for all five cases). In Fig. 12, we compare the results of scattering off the uncoupled ground-state adiabat V_1^{ad} at low energies to those for case I. It is clear that the coupling has resulted in a very slight raising of the effective barrier.[35] After the initial decrease of P_{11} for the coupled potential problems, there are then two sharp peaks due to the two funnel resonances; the energies at which P_{11} reaches unity are in close agreement with the values of E_R. The feature due to funnel resonance 2 is slightly broader than that due to funnel resonance 1, consistent with the larger width for the former. (The complete reflection observed at resonance in the two-state curve-crossing system has been discussed in relation to the topic of molecular switching.[36])

The transition probability P_{11} very nicely illustrates the competition between direct reflection from the diabatic curve V_{11} and metastable trapping (due to resonances). At low scattering energies, below $V_1^{ad,\,max}$, the particle is reflected off the diabat and $P_{11} \approx 1$. As the scattering energy approaches and surpasses the energy of the ground-state adiabatic barrier, the coupling between the diabats lets significant flux pass into channel 4 of the diabat V_{22} and P_{14} approaches unity. However, at the energies of the funnel resonances, P_{14} drops sharply to zero before returning to 1.

All of the delay time plots show two extremely sharp peaks due to the two funnel resonances. There is close agreement, as

Table 5 Energies and partial widths of the funnel resonances

Case	$E_R - V_1^{ad,\,max}$/ cm^{-1}	Γ/ cm^{-1}	Γ_1/ cm^{-1}	Γ_4/ cm^{-1}	$\sum_i \Gamma_i/\Gamma$
Funnel resonance 1					
I	2987.097	20.707	10.36	10.40	1.003
II	3077.288	20.400	10.21	10.24	1.002
III	3177.527	20.053	10.03	10.07	1.002
IV	3277.733	19.700	9.858	9.886	1.002
V	3377.925	19.344	9.680	9.705	1.002
Funnel resonance 2					
I	8680.018	27.361	13.70	13.69	1.001
II	8770.074	26.910	13.48	13.46	1.001
III	8870.168	26.414	13.23	13.21	1.001
IV	8970.236	25.924	12.98	12.97	1.001
V	9070.297	25.439	12.74	12.72	1.001

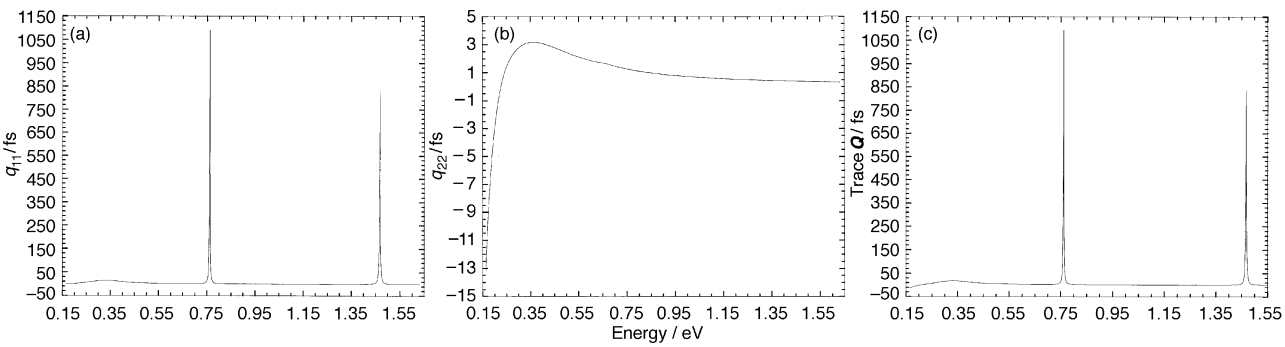

Fig. 11 Same as Fig. 10 but for case V.

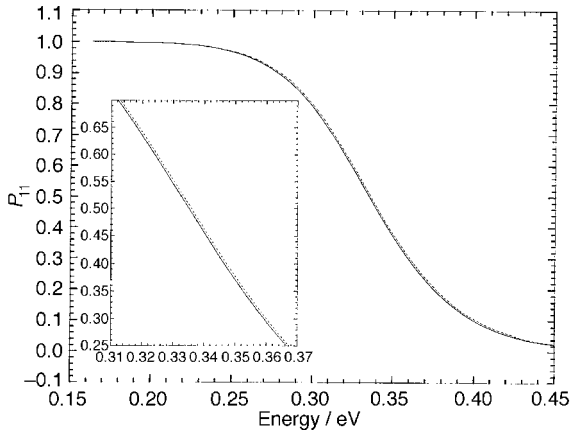

Fig. 12 Transition probability P_{11} at low scattering energies. The solid line is for scattering by the uncoupled adiabatic potential V_1^{ad}, and the dotted line is for scattering by the coupled potentials of case I. The insert shows more clearly that the effective barrier in the coupled case is slightly higher in energy.

seen in Table 6, between the energy of the maximum in Δt_{nm} and the value of E_R of the resonance associated with the delay time feature. For each case, the energies of the local maxima in Δt_{11}, Δt_{14} and Δt_{44} coincide (see Table 3). The first peak of the two has a larger maximum, due to funnel resonance 1 being narrower. Table 6 also gives the product (in units of $\hbar$) of the local maximum in the delay time and the width of the associated resonance. The results in Table 6 are consistent

Table 6 Product (in atomic units) of the resonance width Γ and the local maximum in the delay time at energy E_{max} associated with the resonance energy E_R

Case	E_R/eV	E_{max}/eV	$\Delta t_{11}\Gamma$	$\Delta t_{14}\Gamma$	$\Delta t_{44}\Gamma$
Funnel resonance 1					
I	0.712 794	0.712 80	2.001	2.005	2.009
II	0.723 976	0.723 99	2.001	2.005	2.008
III	0.736 403	0.736 39	2.001	2.004	2.007
IV	0.748 828	0.748 83	2.001	2.004	2.007
V	0.761 250	0.761 24	2.001	2.004	2.006
Funnel resonance 2					
I	1.418 63	1.418 6	2.003	2.002	2.000
II	1.429 79	1.429 8	2.003	2.002	2.000
III	1.442 20	1.44 22	2.003	2.002	2.000
IV	1.454 61	1.454 6	2.003	2.002	2.000
V	1.467 02	1.467 0	2.003	2.002	2.001

Table 7 Ratio of the local maximum in the trace of $\boldsymbol{Q}$ and the local maximum in the delay time Δt_{nm}

Case	Energy/eV	Trace ($\boldsymbol{Q}$)/Δt_{11}	Trace ($\boldsymbol{Q}$)/Δt_{14}	Trace ($\boldsymbol{Q}$)/Δt_{44}
I	0.332 39	[a]	2.000	[a]
	0.712 80	2.004	2.000	1.997
	1.418 6	1.999	2.000	2.001
II	0.332 33		2.000	
	0.723 996	2.004	2.000	1.997
	1.429 8	1.999	2.000	2.001
III	0.332 36		2.000	
	0.736 39	2.003	2.000	1.997
	1.442 2	1.999	2.000	2.001
IV	0.332 33		2.000	
	0.748 83	2.003	2.000	1.998
	1.454 6	1.999	2.000	2.001
V	0.332 36		2.000	
	0.761 24	2.003	2.000	1.998
	1.467 0	1.999	2.000	2.001

[a] Blank entries signify that the maxima in Trace($\boldsymbol{Q}$) and Δt_{nn} did not occur at the same energy.

with our description of the funnel resonances as isolated narrow resonances [see eqn. (13)].

All of the delay times also show a peak of about 9 fs at an energy of 0.33 eV. For this feature, however, the energies of the peaks in the three delay times Δt_{nm} do not coincide as seen from Table 3. However, for a given Δt_{nm}, the values of E_{max}^{nm} and the delay time maximum change insignificantly from case to case. This is consistent with this delay time feature being associated with the maximum in the ground-state adiabatic curve of energy $V_1^{ad,\,max}$. Previous one-dimensional quantum mechanical scattering calculations on *uncoupled* potential energy curves have shown that passage over a potential barrier is associated with a broad barrier resonance.[24] Thus, we conclude that this broad, weak maximum in the delay time at low scattering energies is due to a barrier resonance associated with the maximum in V_1^{ad}. Attempts to locate a pole in the scattering matrix for scattering by the coupled diabats at complex energies (with a real part of 0.33 eV) were not successful; the present numerical algorithm is presumably unable to find resonances so far off the real energy axis, and further investigation is needed. However, we did locate the barrier resonance for scattering off the *uncoupled* ground-state adiabatic curve; the complex resonance energy (in eV) is $0.32742055 - i0.08746875$ in excellent agreement with the analytical result for an unsymmetric Eckart barrier derived by Ryaboy and Moiseyev.[37]

As for the lifetime matrix, the plots of the first eigenvalue q_{11} and the trace of $\boldsymbol{Q}$ show features very similar to those discussed above for the delay time matrix elements. In particular, both display prominent peaks at energies E_R and a broad, weak maximum at lower energies. At the funnel resonance energies (see Table 4), q_{11} is the predominant contributor to the trace; the contribution of q_{22} to the sum at E_R is less than 0.14%. For each case, funnel resonance 1 has a larger value of the trace of $\boldsymbol{Q}$ than funnel resonance 2, and for both resonances the trace of $\boldsymbol{Q}$ increases from case I to case V. The second eigenvalue q_{22} displays a broad, small maximum at low scattering energies and a steep drop-off to negative values at even lower energies. For each case, the trace of $\boldsymbol{Q}$ shows a maximum of 18.1 fs at virtually the same energy; for this feature, q_{22} makes a significant contribution to the sum.

We see from eqn. (13) and (14) that for an isolated narrow resonance in a single channel scattering problem, the ratio of Q to Δt at an energy E_R is two. In Table 7, we have presented the ratio of the trace of $\boldsymbol{Q}$ to the local maximum in Δt_{nm}. For each of the two funnel resonances, which we have noted above are isolated narrow resonances, the maxima in the trace, in the first eigenvalue, and in the delay times coincide in energy, and the ratio of the trace to the delay time is very nearly 2. We should also note that since the second eigenvalue makes a negligible contribution at the funnel resonance energies E_R, the ratio of the first eigenvalue q_{11} to Δt_{nm} will also be very nearly 2. This is consistent with the comment that the eigenvalues, when large, are related to the decay times of metastable states.[28] As for the feature in the trace at low scattering energies, only the maximum in Δt_{14} occurs at the same energy. And, although this feature should be attributed to a broad barrier resonance, even here the ratio of the trace to the delay time is 2, showing that this value of the ratio does not require an extremely narrow resonance.

VI Concluding remarks

We have demonstrated the effect of funnel resonances on transition probabilities and on elements of the delay time and lifetime matrices $\boldsymbol{\Delta t}$ and $\boldsymbol{Q}$ in one-dimensional scattering calculations involving coupled potential energy curves. The funnel resonances produce dramatic changes in the dynamics over a relatively-narrow energy range centered at the resonance energy E_R.

The funnel resonances are closely related to the bound states supported by the *uncoupled* upper adiabatic potential curve. We have computed the bound eigenstates supported by the excited-state adiabat. (These eigenenergies, with respect to the bottom of the well of V_2^{ad}, are invariant to the gap between the two adiabatic potential curves.) The (rotationless) $v = 0$ and $v = 1$ energies are in very close agreement with the (real parts of the) resonance energies of the funnel resonances found in the coupled potential scattering calculations. In particular, the first and second vibrational states are lower than the first and second resonance energy values E_R of case V by 6.930 and 14.465 cm^{-1}, respectively. The $v = 0$ to $v = 1$ splitting is thus within 0.13% of the separation (along the real energy axis) of the two funnel resonance states. The close agreement between the resonance energies E_R and the vibrational eigenstates is consistent with the findings of Qi and Bowman,[18] who analyzed the small differences in their model systems between the energies calculated from the upper adiabat and the resonance positions in terms of the diagonal, nonadiabatic kinetic energy operator. In their earlier work, Baer and Child[16] found oscillatory behavior in the transmission probabilities that was correlated with the position of the eigenvalues in the upper adiabatic curve. Zhu and Nakamura[19–20] also found oscillatory behavior in the transmission probabilities for the nonadiabatic tunneling case; the dramatic features in the transmission probabilities were the narrowest for the strong diabatic coupling regime. (In the present study involving a strong diabatic coupling, we also observe very sharp features in the transmission probabilities.) And, perhaps most significantly, oscillatory behavior has also been seen in three-dimensional reactive scattering.[4]

The funnel resonances characterized in our work can be described as isolated narrow resonances by virtue of (i) the sum of their partial widths being the total width and (ii) the product of the maximum in the delay time and the total width of the associated resonance equalling two. The funnel resonances are clearly responsible for long-lived scattering collisions as evidenced by the large maxima in the sharp delay time features. On the other hand, there are broad, small maxima in the delay times at low scattering energies near the potential maximum of the ground-state adiabat. These short-lived collisions are associated with broad, barrier resonances as studied previously in collinear[24] and three-dimensional scattering. Consistent with the same ground-state adiabat being used in all cases I–V, these delay times features are very similar in magnitude and are found at virtually the same energy for a given Δt_{nm}.

It is interesting to compare some of our one-dimensional results to the three-dimensional quantal calculations of ref. 4. In the full multidimensional study, the funnel resonance occurred at approximately the same energy relative to the minimum of the excited adiabatic surface. From Tables 2 and 5 which give, respectively, the adiabatic gap and the value of E_R referenced to the ground-state adiabatic maximum, we see that the same is true in our reduced-dimensionality study. Secondly, the widths of the first funnel resonance characterized in ref. 4 were close in magnitude to each other; similarly, from Table 5, we see the widths of funnel resonance 1 in all five cases show little variation, as is also true for the widths of funnel resonance 2. Finally, compared to the dynamical calculations carried out on only the ground adiabatic surface, the cumulative reaction probability for the coupled three-dimensional potential surfaces rose from 0 to 1 at a slightly higher energy. Likewise, in our one-dimensional study P_{41}, at low scattering energies, increases from 0 to 1 at a slightly higher energy for the coupled case compared to the uncoupled ground-state adiabat. This behavior was also observed in previous one-dimensional studies.[17,18] Although the comparison between the one- and three-dimensional calculations clearly has limitations, *e.g.*, complete reflections occur at resonance energies in our 1-dimensional cases whereas the multidimensional study of ref. 4 reveals partial reflections at resonance, it is encouraging that the results and conclusions of the full-dimensional studies can be understood in part from our simpler reduced-dimensionality models.

By studying the occurrence of resonances associated with an exciplex funnel situated over a ground-state saddle point, we have provided insight into the conditions responsible for direct reflection of ground-state systems due to diabatic crossing of the saddle point and those responsible for trapping in the exciplex, both of which lower the transmission coefficient for reaction on the ground-state surface.

Acknowledgements

We acknowledge the work of Phillip M. Small, who, as an IPFW undergraduate research assistant, carried out scattering calculations testing the Gram–Schmidt procedure on model potentials. Acknowledgement is made to the Donors of The Petroleum Research Fund, administered by the American Chemical Society, for partial support of this research. This work was also supported by a Purdue Research Foundation Summer Faculty Grant and by the National Science Foundation under grant no. CHE97-25965. Additional support for the computational resources was provided by the Chemistry Department at IPFW.

References

1 M. Gilibert and M. Baer, *J. Phys. Chem.*, 1994, **98**, 12822; 1995, **99**, 15748.
2 G. C. Schatz, *J. Phys. Chem.*, 1995, **99**, 7522; M. H. Alexander, H.-J. Werner and D. E. Manolopoulos, *J. Chem. Phys.*, 1998, **109**, 5710.
3 S. L. Mielke, G. J. Tawa, D. G. Truhlar and D. W. Schwenke, *Chem. Phys. Lett.*, 1995, **234**, 57; S. L. Mielke, D. G. Truhlar and D. W. Schwenke, *J. Phys. Chem.*, 1995, **99**, 16210; M. S. Topaler, T. C. Alison, D. W. Schwenke and D. G. Truhlar, *J. Phys. Chem. A*, 1998, **102**, 1666; M. S. Topaler, T. C. Allison, D. W. Schwenke and D. G. Truhlar, *J. Chem. Phys.*, 1998, **109**, 3321.
4 T. C. Allison, S. L. Mielke, D. W. Schwenke and D. G. Truhlar, *J. Chem. Soc., Faraday Trans.*, 1997, **93**, 825.
5 J. Michl and V. Bonačić-Koutecký, *Electronic Aspects of Organic Photochemistry*, Wiley, New York, 1990.
6 M. Olivucci, I. N. Ragazos, F. Bernardi and M. A. Robb, *J. Am. Chem. Soc.*, 1993, **115**, 3710.
7 S. L. Mielke, G. J. Tawa, D. G. Truhlar and D. W. Schwenke, *J. Am. Chem. Soc.*, 1993, **115**, 6436; S. L. Mielke, G. J. Tawa, D. G. Truhlar and D. W. Schwenke, *Int. J. Quantum Chem. Symp.*, 1993, **27**, 621.
8 I. Yasumori, *Bull. Chem. Soc. Jpn.* 1959, **32**, 1103, 1110.
9 T. C. Allison, G. C. Lynch, D. G. Truhlar and M. S. Gordon, *J. Phys. Chem.*, 1996, **100**, 13575.
10 R. B. Woodward and R. Hoffmann, *The Conservation of Orbital Symmetry*, Verlag Chemie, Weinheim, 1970.
11 W. A. Goddard III, *J. Am. Chem. Soc.*, 1972, **94**, 793.
12 R. A. Marcus, in *Tunneling in Biological Systems*, ed. B. Chance, D. DeVault, H. Fraunfelder, R. A. Marcus, J. R. Schreiffer and N. Sutin, Academic, New York, 1979, p. 109.
13 M. D. Person, P. W. Kash and L. J. Butler, *J. Chem. Phys.*, 1992, **97**, 355; G. C. G. Waschewsky, P. W. Kash, T. L. Myers, D. C. Kitchen and L. J. Butler, *J. Chem. Soc., Faraday Trans.*, 1994, **90**, 1581.
14 I. Wallace, D. J. Funk, J. G. Kaup and W. H. Breckenridge, *J. Chem. Phys.*, 1992, **97**, 3135; S. Bililign, M. D. Morse and W. H. Breckenridge, *J. Chem. Phys.*, 1993, **98**, 2115.
15 L. Landau, *Phys. Z. Sowjetunion*, 1932, **2**, 46; C. Zener, *Proc. R. Soc.*, 1932, **137A**, 696; E. C. G. Stückelberg, *Helv. Phys. Acta*, 1932, **5**, 369; E. E. Nikitin and S. Y. Umanskii, *Theory of Slow Atomic Collisions*, Springer-Verlag, Berlin, 1984; H. Nakamura, *Int. Rev. Phys. Chem.*, 1991, **10**, 123; H. Nakamura, *Annu. Rev. Phys. Chem.*, 1997, **48**, 299; H. Nakamura, in *Dynamics of Molecules and Chemical Reactions*, ed. R. E. Wyatt and J. Z. H. Zhang, Dekker, New York, 1996, p. 473.
16 M. Baer and M. S. Child, *Mol. Phys.*, 1978, **36**, 1449.
17 S. Shin and J. C. Light, *J. Chem. Phys.*, 1994, **101**, 2836.

18 J. Qi and J. M. Bowman, *J. Chem. Phys.*, 1996, **104**, 7545.
19 C. Zhu and H. Nakamura, *J. Chem. Phys.*, 1993, **98**, 6208; 1994, **101**, 4855.
20 C. Zhu and H. Nakamura, *J. Chem. Phys.*, 1994, **101**, 10630.
21 C. Zhu and H. Nakamura, *J. Chem. Phys.*, 1997, **107**, 7839.
22 H. Nakamura, *J. Chem. Phys.*, 1987, **87**, 4031.
23 D. C. Chatfield, R. S. Friedman, D. G. Truhlar and D. W. Schwenke, *Faraday Discuss. Chem. Soc.*, 1991, **91**, 289; D. C. Chatfield, R. S. Friedman, D. W. Schwenke and D. G. Truhlar, *J. Phys. Chem.*, 1992, **96**, 2414.
24 R. S. Friedman and D. G. Truhlar, *Chem. Phys. Lett.*, 1991, **183**, 539; R. S. Friedman, V. D. Hullinger, and D. G. Truhlar, *J. Phys. Chem.*, 1995, **99**, 3184.
25 A. Messiah, *Quantum Mechanics*, Wiley, New York, 1966.
26 J. R. Taylor, *Scattering Theory*, Wiley, New York, 1972; R. G. Newton, *Scattering Theory of Particles and Waves*, Springer-Verlag, New York, 2nd edn., 1982.
27 M. V. Basilevsky and V. M. Ryaboy, *Int. J. Quantum Chem.*, 1981, **19**, 611.
28 F. T. Smith, *Phys. Rev.*, 1960, **118**, 349; F. T. Smith, *J. Chem. Phys.*, 1962, **36**, 248.
29 A. M. Lane and R. G. Thomas, *Rev. Mod. Phys.*, 1958, **30**, 257; J. Humblet and L. Rosenfeld, *Nucl. Phys.*, 1961, **26**, 529; H. A. Weidenmüller, *Ann. Phys.* (*NY*), 1964, **28**, 60; 1964, **29**, 378.
30 D. W. Schwenke and D. G. Truhlar, *J. Chem. Phys.*, 1987, **87**, 1095; R. S. Friedman and D. G. Truhlar, in *Multiparticle Quantum Scattering with Applications to Nuclear, Atomic and Molecular Physics*, ed. D. G. Truhlar and B. Simon, Springer, New York, 1997, p. 243.
31 M. E. Riley and A. Kuppermann, *Chem. Phys. Lett.*, 1968, **1**, 537.
32 A. C. Allison, *J. Comput. Phys.*, 1970, **6**, 378.
33 W. H. Press, B. P. Flannery, S. A. Teukolsky and W. T. Vetterling, *Numerical Recipes*, Cambridge University Press, Cambridge, 1986.
34 R. T. Skodje, D. W. Schwenke, D. G. Truhlar and B. C. Garrett, *J. Phys. Chem.*, 1984, **88**, 628; R. T. Skodje, D. W. Schwenke, D. G. Truhlar and B. C. Garrett, *J. Chem. Phys.*, 1984, **80**, 3569.
35 B. C. Garrett and D. G. Truhlar, *J. Chem. Phys.*, 1985, **82**, 4543.
36 H. Nakamura, *J. Chem. Phys.*, 1992, **97**, 256; S. Nanbu, H. Nakamura and F. O. Goodman, *J. Chem. Phys.*, 1997, **107**, 5445.
37 V. Ryaboy and N. Moiseyev, *J. Chem. Phys.*, 1993, **98**, 9618.

Paper 8/08516A